Functional disorders of the sympathetic nervous system in mice lacking the α_{1B} subunit (Ca_v 2.2) of N-type calcium channels

Mitsuhiro Ino*†, Takashi Yoshinaga*†, Minoru Wakamori‡, Norimasa Miyamoto*, Eiki Takahashi*, Jiro Sonoda*, Takaki Kagaya*, Tohru Oki*, Takeshi Nagasu*, Yukio Nishizawa*, Isao Tanaka*, Keiji Imoto‡, Shinichi Aizawa§, Sheryl Koch¶, Arnold Schwartz¶, Tetsuhiro Niidome*, Kohei Sawada*‖, and Yasuo Mori‡

*Tsukuba Research Laboratories, Eisai Co., 5-1-3 Tokodai, Tsukuba, Ibaraki 300-2635, Japan; ‡Department of Information Physiology, National Institute for Physiological Sciences, Myodaiji, Okazaki, Aichi 444-8585, Japan; §Department of Morphogenesis, Institute of Molecular Embryology and Genetics, Kumamoto University, Kumamoto University School of Medicine, 2-2-1, Honjo, Kumamoto 860, Japan; and ¶Institute of Molecular Pharmacology and Biophysics, University of Cincinnati, College of Medicine, Cincinnati, OH 45267-0828

Communicated by Bert Sakmann, Max Planck Institute for Medical Research, Heidelberg, Germany, February 21, 2001 (received for review November 2, 2000)

N-type voltage-dependent Ca^{2+} channels (VDCCs), predominantly localized in the nervous system, have been considered to play an essential role in a variety of neuronal functions, including neurotransmitter release at sympathetic nerve terminals. As a direct approach to elucidating the physiological significance of N-type VDCCs, we have generated mice genetically deficient in the α_{1B} subunit (Ca_v 2.2). The α_{1B}-deficient null mice, surprisingly, have a normal life span and are free from apparent behavioral defects. A complete and selective elimination of N-type currents, sensitive to ω-conotoxin GVIA, was observed without significant changes in the activity of other VDCC types in neuronal preparations of mutant mice. The baroreflex response, mediated by the sympathetic nervous system, was markedly reduced after bilateral carotid occlusion. In isolated left atria prepared from N-type-deficient mice, the positive inotropic responses to electrical sympathetic neuronal stimulation were dramatically decreased compared with those of normal mice. In contrast, parasympathetic nervous activity in the mutant mice was nearly identical to that of wild-type mice. Interestingly, the mutant mice showed sustained elevation of heart rate and blood pressure. These results provide direct evidence that N-type VDCCs are indispensable for the function of the sympathetic nervous system in circulatory regulation and indicate that N-type VDCC-deficient mice will be a useful model for studying disorders attributable to sympathetic nerve dysfunction.

Voltage-dependent Ca^{2+} channels (VDCCs) mediate calcium entry into cells, which is essential for a wide variety of physiological functions. Among three types of VDCCs, P/Q-type, N-type, and R-type, predominantly expressed in neuronal cells (1, 2), N-type Ca^{2+} channels have been recognized as high-voltage-activated Ca^{2+} channels selectively sensitive to blockade by ω-conotoxin GVIA (ω-CTX), a 27-amino acid peptide isolated from the venom of the fish-hunting cone snail *Conus geographus*, but resistant to the L-type Ca^{2+} channel-specific blockers such as dihydropyridines. Molecular studies have revealed that the α_{1B} (Ca_v2.2) subunit gene encodes N-type Ca^{2+} channels and is expressed widely in neuronal tissues (3–12). Experiments employing ω-CTX have demonstrated the physiological significance of the N-type Ca^{2+} channels in the nervous system, where they have a specific developmental role in the migration of immature neurons before the establishment of their synaptic circuit (13). N-type Ca^{2+} channels have been shown to be critically involved in the release of neurotransmitters, including glutamate (14–16), γ-aminobutyric acid (14), acetylcholine (17), dopamine (18–20), and norepinephrine (21) in mammalian central neurons. For instance, in CA1 hippocampal neurons, the inhibitory GABAergic synaptic potentials are reduced by 85–90% by saturating concentrations of ω-CTX, whereas the excitatory glutaminergic transmission is blocked by 65–70% (16).

In peripheral neurons such as autonomic neurons and motor neurons and in spinal cord neurons, N-type Ca^{2+} channels have been suggested to contribute to the release of neurotransmitters from nerve terminals (22). The blockade of Ca^{2+} currents by ω-CTX showed a potent antinociceptive effect (23), because many of the nerve terminals expressing the N-type Ca^{2+} channels contain the nociceptive peptide substance P (12). In guinea pig trachea, acetylcholine release caused by electrical stimulation was inhibited by ω-CTX. ω-CTX also inhibited neurotransmitter release in cultured rat sympathetic neurons (22, 24) and in anesthetized cat heart (25, 26). Furthermore, ω-CTX suppressed the sympathetic nerve-mediated positive-inotropic effects in isolated guinea pig atria (27–29) and blocked sympathetic cardiac efferent activity in conscious rabbits (30). These results suggest that N-type Ca^{2+} channels play important roles in both the central and peripheral nervous systems. However, considering that ω-CTX is a relatively large polypeptide with limited distribution into tissues and that it does also inhibit certain L-type Ca^{2+} channels in neurons (31, 32), an alternative direct approach is necessary to elucidate in detail the *in vivo* functions of N-type Ca^{2+} channels.

Recently, genetically engineered mice lacking the α_{1A} (P/Q-type) (33), α_{1E} (R-type) (34), α_{1c} (L-type) (35), or α_{1D} (L-type) (36) subunit have been developed to clarify the *in vivo* functions of P/Q-type, R-type, or L-type Ca^{2+} channels. The α_{1A} subunit-deficient mice exhibit a rapidly progressive neurological deficit with specific characteristics of ataxia and dystonia before dying within 3–4 weeks after birth. The α_{1E} subunit mutant mice show attenuation of the inhibitory effect of the descending antinociceptive pathway, causing abnormalities in pain responses. The α_{1D} subunit-deficient mice lack L-type currents in cochlear inner hair cells, causing deafness, and show dysfunction of the sinoatrial node, suggesting that the α_{1D} subunit is essential for normal auditory function and regulation of cardiac pacemaker activity. Thus a genetic approach is extremely effective in elucidating the physiological functions of the respective VDCC types. In this study we have explored the physiological significance of N-type Ca^{2+} channels by creating genetically engineered mice lacking the α_{1B} subunit. The results indicate that genetic elimination of N-type Ca^{2+} channels leads to specific

PHYSIOLOGY

Abbreviations: VDCC, voltage-dependent Ca^{2+} channel; ω-CTX, ω-conotoxin GVIA; ES, embryonic stem; AP, atrial pressure; mAP, mean AP; HR, heart rate; EFS, electrical field stimulation; SCG, superior cervical ganglion.

†M.I. and T.Y. contributed equally to this work.

‖To whom reprint requests should be addressed. E-mail: k-sawada@hhc.eisai.co.jp.

The publication costs of this article were defrayed in part by page charge payment. This article must therefore be hereby marked "*advertisement*" in accordance with 18 U.S.C. §1734 solely to indicate this fact.

deficits in the sympathetic regulation of the circulatory system, suggesting that this strain will be useful for studying the mechanism of neurotransmission and autonomic failure.

Materials and Methods

Generation of Knockout Mice of α_{1B} Subunit of VDCCs. A genomic DNA clone with the coding exons was isolated from the λFIXII library prepared from genomic DNA of 129SVJ mice (Stratagene) with the use of a suitable probe. The probe (a 0.7-kb cDNA fragment), which corresponds to the cytosol region from 2,476 to 3,167, was amplified with primer set B3–1 (5′-TTGTACAGTGAGATGGACCCTGAGGAGC-3′) and B3–2 (5′-GGCCTCCAGGTCACAGTGAGGTTCCTTGGG-3′). The phosphoglycerol kinase promoter neomycin resistance cassette was inserted between the 5′ homology region (3.1 kb) and the 3′ homology region (6.7 kb) at the *Aat*II restriction enzyme site of the genomic DNA clone, which was subcloned to the thymidine kinase cassette of pBluescript SK+ (Stratagene). The constructed targeting vector contained sequences identical to those of the mouse genome, except for the interruption by the positive selection marker, the phosphoglycerol kinase promoter neomycin resistance cassette.

The constructed targeting vector was electroporated into TT2 embryonic stem (ES) cells (37). Gene targeting was screened by Southern blotting with the use of two 5′ probes, one out of the targeting region and the other in an internal homologous region. Gene-targeted ES cell clones were injected into fertilized eggs at the eight-cell stage of ICR mice. Chimeric male mice were mated with C57BL/6 females, and heterozygous male and female mice were interbred to generate mice in which the α_{1B} subunit of VDCCs was knocked out.

Southern Blot Analysis. Genotyping of tail DNA was performed by Southern blot analysis. *Bam*HI-digested DNA was probed with isolated genomic DNA (Pro N) obtained from *Nco*I digestion.

Reverse Transcription–PCR. The expression pattern of mRNA in the brain was confirmed by reverse transcription–PCR. After the synthesis of complementary DNAs from total RNAs with SuperScript II reverse transcriptase (Life Technologies, Rockville, MD) with an oligo(dT) primer, the fragments were amplified with primer sets P1 (5′-CCAGACATGAAGACACACATGGAC-3′) and P3 (5′-GCCTGTCAGTGTCACTGGGACATGCACACAGT-3′) for the detection of the wild-type mRNA, or primer sets P2 (5′-ATGCTCCAGACTGCCTTGGGAAAAGCGCCT-3′) and P3 for mutant mRNA. The predicted fragment sizes from the wild type and the mutant were 764 bp and 509 bp, respectively.

Northern Blot Analysis. Northern blot analysis of the α_{1B} subunit of N-type VDCCs in the brain was carried out with the use of the 0.7-kb cDNA probe prepared in phage clone screening. Total RNA was prepared from brain tissue by the acid guanidinium-phenol-chloroform method. Poly(A)$^+$ was purified by oligo(dT) column chromatography, according to the manufacturer's instructions (Amersham Pharmacia). Poly(A)$^+$ RNA (5 μg per lane) was electrophoresed through a 0.5% formaldehyde-agarose gel and transferred to a nylon membrane (DuPont/NEN). Radiolabeled probe was hybridized overnight in ExpressHyb (CLONTECH).

Electrophysiological Study by Whole-Cell Recording. Electrophysiological measurements were performed on dorsal root ganglion and superficial cervical ganglion. Currents were recorded at room temperature (22–25) with the use of the whole-cell mode of the patch-clamp technique (38) with an Axopatch 200B patch-clamp amplifier (Axon Instruments, Foster City, CA). Patch pipettes were made from borosilicate glass capillaries (1.5 mm outer diameter, 1.1 mm inner diameter; Narishige, Tokyo) with a model P-87 Flaming-Brown micropipette puller (Sutter Instruments, San Rafael, CA). The patch electrodes were fire-polished. Resistance ranged from 1 to 2 MΩ when the pipettes were filled with the pipette solutions described below. The series resistance was electronically compensated to >70%, and both the leakage and the remaining capacitance were subtracted by the -P/6 method. Currents were sampled at 10 kHz after low-pass filtering at 2 kHz (−3 dB) with the use of an 8-pole Bessel filter (model 900; Frequency Devices, Haverhill, MA). Data were collected and analyzed with PCLAMP 6.02 software (Axon Instruments). Ba^{2+} currents were recorded in an external solution that contained (in mM) 3 $BaCl_2$, 155 tetraethylammonium chloride, 10 Hepes, and 10 glucose (pH adjusted to 7.2 with tetraethylammonium hydroxide). The pipette solution contained (in mM) 85 cesium-aspartate, 40 CsCl, 2 $MgCl_2$, 5 EGTA, 2 MgATP, 5 Hepes, and 10 creatine phosphate (pH adjusted to 7.4 with CsOH). In the experiments with ω-agatoxin IVA (0.1 μM), ω-CTX (1 μM), and nimodipine (10 μM), the external solution was always supplemented with 0.1 mg/ml cytochrome *c*. Cytochrome *c* at 0.1 mg/ml had no effect on Ba^{2+} currents. Rapid application of drugs was achieved by using a modified "Y-tube" method (38). The external solution surrounding a recorded cell was completely exchanged within 200 ms.

Measurement of Atrial Pressure and Heart Rate. Mice were anesthetized with urethane (1.5 g/kg, i.p.). The throat was incised, and polyethylene tubing (PE-10; Becton Dickinson) filled with PBS containing 100 units heparin/ml was inserted into the right common carotid artery and connected to a microtip catheter pressure transducer (PM-500; Millar Instruments, Houston, TX). Pulsatile pressure and mean arterial blood pressure were recorded on a thermal array recorder (RTA-1100 M; Nihon Koden, Tokyo) via a carrier amplifier (AP-601G; Nihon Koden). The heart rate was calculated with a tachometer triggered by pulse pressure with the use of a heart rate counter (AT-601G; Nihon Koden). Another stretched PE-10 catheter was inserted into the right jugular vein for administration of ω-CTX. The left carotid artery was ligated for 30 s with 6–0 silk sutures to observe the baroreflex responses. The preparation was allowed to stabilize for at least 30 min before the start of the experiment.

Inotropic Responses to Electrical Field Stimulation. The wild-type and knock-out mice were killed by cervical dislocation. The heart was rapidly removed and placed in oxygenated Tyrode's solution (see below) at room temperature. The left atrium was then dissociated, and contractile force was measured with a forth displacement transducer (CD200; Nihon Koden) at 37°C. The Tyrode's solution contained (in mM) 123.8 NaCl, 5.0 KCl, 2.0 $CaCl_2$, 1.2 $MgCl_2$, 25.0 $NaHCO_3$, and 11.2 glucose.

Isolated left atria were stimulated at 2 Hz with a voltage just above the threshold for basal contraction (1-ms duration) for 30 min to stabilize the basal contraction. Thereafter 4 field pulses (0.1-ms duration, 1.5 times basal stimulation voltage, 200 Hz) were applied in each basic stimulation for 15 s for sympathetic or parasympathetic nerve stimulation. To assess responses to sympathetic or parasympathetic nerve stimulation, atria were perfused with 1 μM atropine or 1 μM propranolol, respectively.

Norepinephrine Plasma Levels. Blood samples were collected from mice anesthetized with urethane (1.5 g/kg, i.p.). At 30 min after the anesthesia induction, 400 μl of blood was drawn from the left artery with a syringe containing EDTA/2Na (0.37 mg/ml) and centrifuged. Plasma (200 μl) combined with saline (200 μl), activated alumina (50 mg), and 3,4-dihydroxybenzylamine (2.5 ng) as an internal standard was rotated for 1.5 h at 4°C. The alumina was washed with chilled distilled water three times, then plasma norepinephrine was extracted with 0.1 M perchloric acid

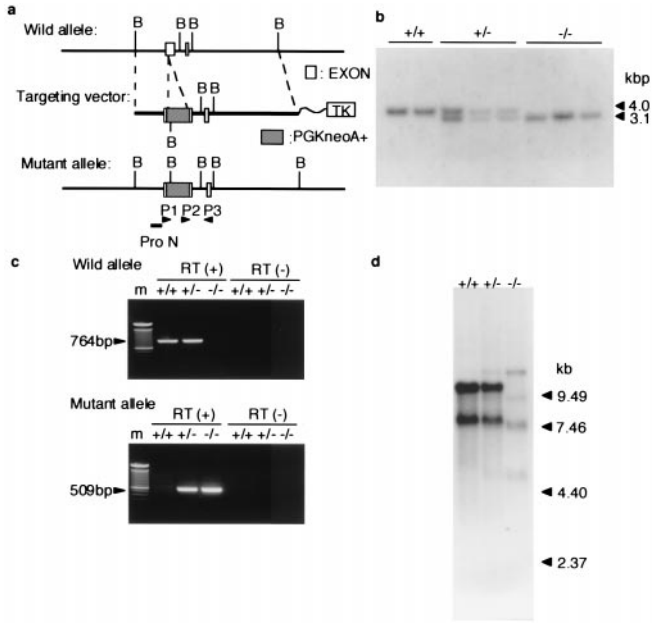

Fig. 1. Generation and characterization of mice lacking a functional α_{1B} gene. (*a*) Strategy for gene disruption. B, *Bam*HI site. (*b*) Southern blot analysis. Tail DNAs derived from heterozygous progeny were digested with *Bam*HI. +/+, wild-type mice; 4.0 kb, KO mice (−/−); 3.1 kb, heterozygous mice (+/−). (*c*) Reverse transcription–PCR analysis of total brain RNA showed an alteration in fragment size. (*Upper*) Wild primer pair (P1 + P3). (*Lower*) Mutant primer pair (P2 + P3). m, 100-bp ladder. (*d*) Northern blot analysis of mouse poly(A)$^+$ RNA demonstrates the absence of α_{1B} mRNA in the brain of KO mice.

(200 μl) and quantified by HPLC with electrochemical detection as described previously (39).

Data Analysis. Values are expressed as means ± SE. Statistical comparison was performed with Student's *t* test (*, $P < 0.05$; **, $P < 0.01$; ***, $P < 0.001$).

Results

Creation of α_{1B} Subunit-Deficient Mice. To disrupt the α_{1B} subunit gene, phosphoglycerol kinase promoter neomycin resistance cassette was fused with the genomic exon that encodes the central portion of the cytoplasmic repeat II–III linker, in the reverse direction (Fig. 1*a*). Linearized targeting vector was electroporated into ES cells, and targeted ES cells were screened. Nine of 116 clones were identified as targeted ES cells by Southern blot analysis. Chimeric mice were generated from three of five clones independently and backcrossed to C57BL/6. Homozygous mice obtained from heterozygotes were intercrossed to obtain homozygous mice (−/−). The offspring from heterozygote mating were 22.4% (54/241) wild type, 53.1% (128/241) heterozygous mutant, and 24.5% (59/241) homozygous mutant, the genotypes of which were determined by Southern blot analysis with the use of the genomic DNA (Fig. 1*b*). The ratio fits that expected from Mendelian theory by χ^2 analysis, surprisingly suggesting that the disruption of the α_{1B} subunit of N-type Ca^{2+} channels is not embryonic-lethal. Reverse transcription–PCR assay confirmed the absence of normal α_{1B} RNA transcripts and the presence of disrupted transcripts in the brain of mutant mice (Fig. 1*c*). Northern blotting revealed two normal α_{1B} transcripts (8.5 and 10.3 kb) in the brain (6) from wild-type and heterozygous mice, but only extremely low-level expression of the aberrant 11.5-kb transcript, which represents the α_{1B} RNA transcript disrupted by insertion of the antisense sequence of the neomycin cassette, in homozygous mutant mice

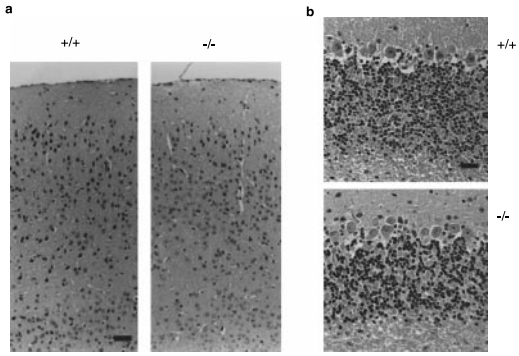

Fig. 2. Histological analyses of brain in α_{1B}-deficient mice. Cerebral cortex (*a*) and cerebellum (*b*) obtained from the mice (20 weeks) were dissected and stained with hematoxylin/eosin. [Bars: 50 μm (cerebral cortex) and 25 μm (cerebellum).]

(Fig. 1*d*). The homozygous mutant mice were alive after more than a year without apparent behavioral defects and were capable of producing offspring with a normal litter size. In the cerebral cortex, the anatomical-histological features in neuron, glias (including astrocytes, oligodendrocytes, and microglias), and endothelial cells were indistinguishable between the wild mice and the mutant mice (6-20 w) (Fig. 2). The sizes and cell density of the granule cell layer, the Purkinje cell layer, and the molecular cell layer in the cerebellum of mutant mice appeared normal in their cell number, shape, and anatomical arrangement. Furthermore, no obvious changes were found in heart, kidney, lung, liver, or spleen of mutant mice (data not shown).

Ablation of N-Type Ca^{2+} Currents in Neurons of Superior Cervical Ganglion. Sympathetic neurons are a useful system in which to quantitatively relate VDCC activity with the downstream cellular response, i.e., neurotransmitter release (22). Deficit of the α_{1B} subunit caused a significant reduction in the total Ba^{2+} current density (45.5 ± 3.9 pA/pF, $n = 15$) in neurons of the superior cervical ganglion (SCG) of mutant mice compared with wild-type mice (73.7 ± 3.8 pA/pF, $n = 15$, $P < 0.001$). We determined the relative contribution of N-type Ca^{2+} channel current to the total Ca^{2+} channel currents in SCG neurons. Electrophysiological recordings demonstrated the coexistence of L, N, and P/Q types, distinguished by dihydropyridines, ω-CTX, and ω-agatoxin IVA, respectively, and the residual R type in each neuron. L-, P/Q-, and R-type VDCCs are encoded by the α_{1C} or α_{1D}, α_{1A}, and α_{1E} gene, respectively. SCG neurons from wild-type mice showed large ω-CTX-sensitive N-type currents (32.6 ± 3.2 pA/pF, $n = 15$) that did not recover from blockade by ω-CTX upon washout, whereas N-type current was only marginal in α_{1B}-deficient mice (0.7 ± 0.3 pA/pF, $n = 15$). In contrast to the N-type current, the L-type component sensitive to the dihydropyridine derivative nimodipine and the P-type current component blocked by 0.1 μM ω-agatoxin IVA were unaffected by the disruption of the α_{1B} subunit gene (Fig. 3). These results indicate that the reduction of total Ca^{2+} channel currents is due to elimination of the ω-CTX-sensitive N-type current in deficient mice and that compensation for the reduced current fraction by other types of Ca^{2+} channels was absent in SCG neurons of deficient mice. Similar selective elimination of N-type currents by α_{1B} gene disruption was observed in other neuronal preparations, such as dorsal root ganglion cells (data not shown).

Chronic Elevation of Blood Pressure and Heart Rate Is Insensitive to Administration of ω-Conotoxin GVIA. It has been reported that administration of ω-CTX causes hypotension in rabbits and

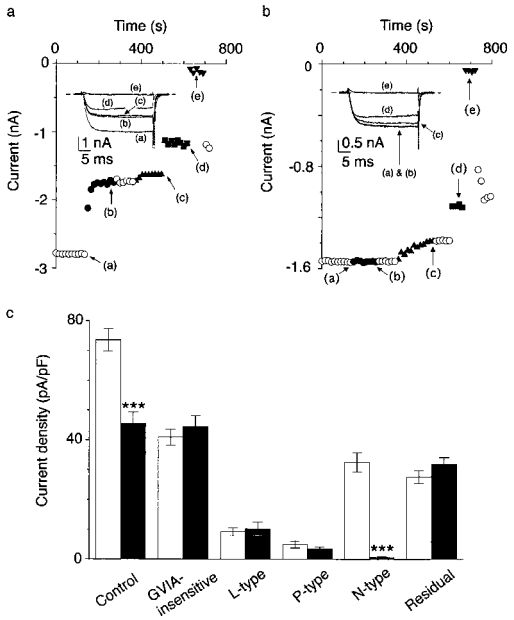

Fig. 3. Selective elimination of N-type channel current in SCG neurons of α_{1B}-deficient mice. (*a* and *b*) Effects of 1 μM ω-CTX (●), 0.1 μM ω-agatoxin IVA (▲), 10 μM nimodipine (■), and 10 μM Cd^{2+} (▼) on Ba^{2+} currents in wild-type mice (*a*) and knock-out mice (*b*). (*Insets*) Representative current traces activated by depolarization for 30 ms to 5 mV from a V_h of −80 mV. (*c*) Histogram of current density in wild-type mice (open bar) and KO mice (solid bar). Data are expressed as means ± SE of 15 SCG neurons.

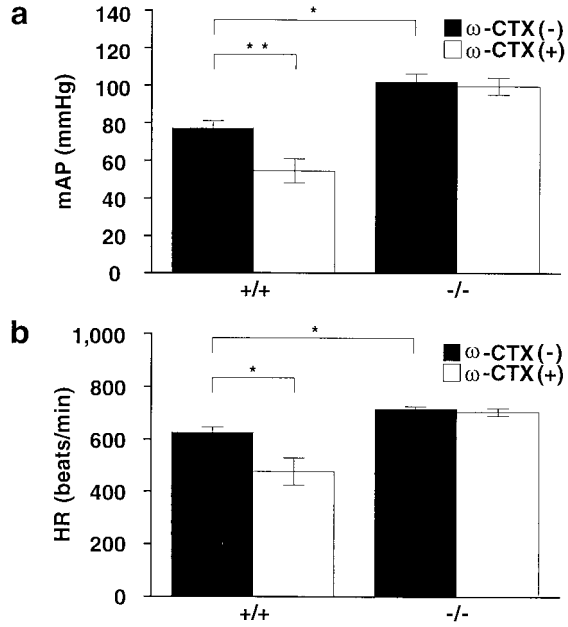

Fig. 4. Response of mean arterial pressure and heart rate to (*a* and *b*) ω-CTX. Summarized results of mean arterial pressure (*a*) and heart rate (*b*) in the absence (solid column) or presence (open column) of ω-CTX (30 μg/kg) in wild-type and KO mice. mAP and HR were measured 30 min after administration of ω-CTX. Data are expressed as means ± SE.

guinea pigs (30, 40), and therefore we measured arterial blood pressure (AP) and heart rate (HR) through a catheter placed in the carotid artery in anesthetized mice. A group of five animals (13–15 weeks) weighing 31.6 ± 8.2 g and 31.5 ± 3.8 g for wild and knock-out mice, respectively, were used. Surprisingly, under the control condition, mean AP (mAP) and HR in knock-out mice were 102.0 ± 4.3 mmHg and 714.0 ± 11.5 beats per minute, respectively, which are significantly higher than those in wild-type mice (77.0 ± 3.9 mmHg and 625.4 ± 20.0 beats per minute; Fig. 4). Administration of ω-CTX (30 μg/kg) decreased significantly the mAP by 22.6 ± 2.6 mmHg and HR by 158.4 ± 41.3 beats per minute in wild-type mice after 30 min, but exerted only marginal effects on mAP and HR in knock-out mice (2.4 ± 1.0 mmHg and 10.3 ± 7.0 beats per minute). These results clearly demonstrate that the genetic deficit of N-type VDCCs leads to higher levels of mAP and HR, suggesting abnormalities in the regulation of cardiovascular function in N-type-deficient mice.

Abnormalities of Bilateral Carotid Artery Occlusion Response. To assess sympathetic nerve function in knock-out mice, we first studied the carotid baroreflex function. The baroreceptors located in carotid sinus detect changes in aortic blood pressure and regulate blood pressure through the activation of sympathetic or parasympathetic nerve via the central nervous system (solitary nucleus, C1 region, and intermedius lateral column). When bilateral carotid artery is occluded, the blood pressure in the carotid sinus decreases, and activation of sympathetic nerve is triggered to increase blood pressure. We measured the change in mAP in response to bilateral carotid artery occlusion under anesthesia (41). Fig. 5 summarizes the change in mAP at the end of bilateral carotid artery occlusion (30 s). In wild-type mice, mAP was increased by bilateral carotid artery occlusion (21.7 ± 5.2 mmHg, $n = 5$), and this baroreflex was significantly suppressed by 30 μg/kg of ω-CTX (5.8 ± 1.2 mmHg, $P < 0.05$). On the other hand, in knock-out mice, only a slight increment of AP was observed (7.6 ± 2.1 mmHg, $n = 5$), and the change was unaffected by ω-CTX. The change in mAP via baroreflex in α_{1B}-deficient mice was not significantly different from the change in wild-type mice treated with ω-CTX, revealing a lack of compensation by VDCC types other than N in the mutant mice. These results demonstrate that carotid baroreflex function, predominantly mediated by N-type VDCCs in wild-type mice, was greatly impaired in N-type knock-out mice.

Impaired Inotropic Contraction in Isolated Left Atria. Because the possibility that sustained up-regulation of sympathetic activity impairs baroreflex and maintains high basal mAP and HR in N-type-deficient mice cannot be excluded, we next assessed sympathetic nerve activity directly by measuring inotropic responses to electrical field stimulation (EFS) in isolated left atria. The contractile force of atria is modulated by both sympathetic nerve and parasympathetic nerve in opposite directions. Norepinephrine released from sympathetic nerve endings increases

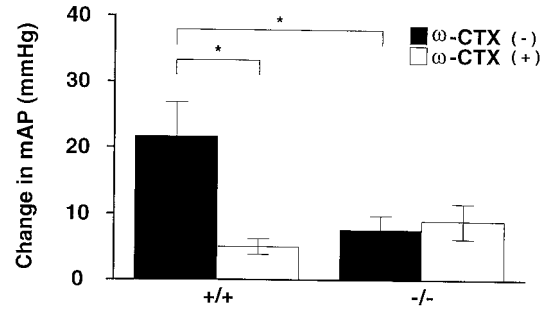

Fig. 5. Attenuation of vascular and cardiac sympathetic activities in N-type KO mice. Shown are the summarized results of blood pressure responses to bilateral carotid artery occlusion in the absence (solid column) or presence (open column) of ω-CTX in wild-type and KO mice. Each column represents the mean ± SE of five experiments.

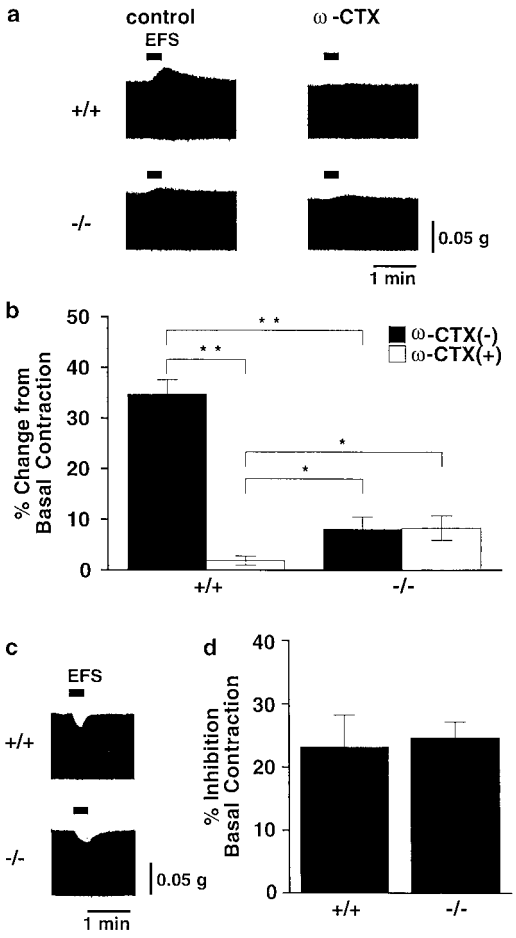

Fig. 6. Positive and negative inotropic responses to electrical field stimulation (EFS). (*a*) Representative records of positive inotropic responses to EFS in the absence (*Left*) or presence (*Right*) of ω-CTX (30 nM) in wild-type mice (*Upper*) and in N-type Ca^{2+} channel-deficient mice (*Lower*). Experiments were carried out in the presence of atropine (1 μM). (*b*) Summarized results of the sympathetic nerve-mediated positive inotropic responses in the presence or absence of ω-CTX. Each column represents the mean ± SE of five experiments. (*c*) Representative records of negative inotropic responses to EFS in wild-type mice (*Upper*) or KO mice (*Lower*). Experiments were carried out in the presence of propranolol (1 μM). (*d*) Summarized results of the parasympathetic nerve-mediated negative inotropic responses. Each column represents the mean ± SE of five experiments.

the contractile force through the β-adrenergic receptor stimulation, leading to calcium channel current potentiation, whereas acetylcholine released from the parasympathetic nerve endings decreases the contractile force via the muscarinic acetylcholine receptor stimulation, leading to the activation of G-protein-gated inwardly rectifying K channels. Therefore, an antimuscarinic (anticholinergic) agent atropine or an adrenergic receptor blocker propranolol was used to examine separately the function of sympathetic or parasympathetic nerve activity, respectively (29). A positive inotropic response that was abolished after treatment with ω-CTX (30 nM) was induced by EFS in atria of wild-type mice in the presence of atropine (Fig. 6*a, Upper*). In contrast to wild-type mice, only a slight increment of contractile force, which was unaffected by ω-CTX, was induced by EFS in knock-out mice (Fig. 6*a, Lower*). The positive inotropic response to EFS in the left atrium of wild-type mice (34.7 ± 5.9% change from basal contraction, $n = 5$) was significantly higher than that of knock-out mice (8.1 ± 2.4% change from basal contraction, $n = 5$; Fig. 6*b*). In the presence of ω-CTX, the positive inotropic response in knock-out mice (8.3 ± 2.4%) was significantly higher than that in wild-type mice (1.9 ± 0.9%), suggesting that some compensatory mechanism strengthens the atrial contraction. Because autonomic regulation of blood pressure includes parasympathetic regulation as an important mechanism, we also examined the activity of parasympathetic neurons in wild-type and knock-out mice by measuring the negative inotropic responses to EFS in atria in the presence of propranolol (1 μM) (Fig. 6*c*). The amplitudes of negative inotropic responses to EFS were indistinguishable between wild-type mice (23.2 ± 5.0%, $n = 5$) and knock-out mice (24.6 ± 2.5%, $n = 5$, Fig. 6*d*). The positive inotropic response induced by EFS should reflect the amount of norepinephrine released from sympathetic nerve endings, because the positive inotropic response was completely blocked by tetrodotoxin (sodium channel blocker, 0.1 μM) or propranolol, and the atrial muscles of wild-type and knock-out mice showed similar sensitivities to externally applied isoproterenol (β-adrenergic-receptor agonist) and propranolol (data not shown).Furthermore, the heart-weight/body-weight ratio of knock-out mice (0.551 ± 0.017%, $n = 10$) showed no obvious difference from that of wild-type mice at 20 weeks of age (0.561 ± 0.014%, $n = 10$), i.e., there was no indication of heart failure in mutant mice, although abnormal activity of the sympathetic nervous system has been implicated in the pathogenesis of heart failure (42, 43). These results suggest that the neurotransmitter release in sympathetic nerve terminals in wild-type mice is controlled by N-type VDCCs, the contribution of which is only slightly compensated for by other types in knock-out mice, but that parasympathetic nerve activity is regulated by types other than N-type VDCCs.

Discussion

The present investigation has demonstrated selective elimination of N-type VDCC activity in SCG neurons and sympathetic nerve terminals in α_{1B}-deficient mice, in which sympathetic nerve activity was markedly diminished but parasympathetic nerve activity was unaffected. The results obtained with genetically engineered deficient mice provide direct evidence that the function of the sympathetic nervous system is predominantly regulated by N-type VDCCs *in vivo*, strongly suggesting that the essential role of N-type Ca^{2+} channels cannot be filled by other VDCC types present in mutant SCG neurons. The N-type gene disruption did not cause apparent developmental defects of sympathetic neurons, in contrast to deficiency of the homeobox gene Phox2b (44) and dopamine β-hydroxylase (essential for noradrenaline synthesis; ref. 45), or trophic effects that would induce denervation hypersensitivity in organs, such as the heart, that are innervated by sympathetic neurons. Surprisingly, the N-type-deficient mice appeared to have a normal life span without apparent behavioral defects, although our initial expectation had been that N-type deficiency would be associated with severe behavioral abnormality or even embryonic lethality, inasmuch as previous studies have demonstrated important contributions of N-type channels to the evocation of essential cellular responses in both the peripheral and central nervous systems (3, 5–12, 22). It is therefore possible that other types can substitute for the N-type Ca^{2+} channels in inducing certain neuronal processes, in contrast to the essential role played by the N-type Ca^{2+} channels in sympathetic nerve activity. Phenotypes in other tissues such as brain and sensory neurons, where N-type channels are distributed, should also be studied systematically in N-type knock-out mice.

Importantly, the knock-out mice showed elevated basal mAP despite sympathetic nerve dysfunction, which is an interesting observation, because mAP and HR should be decreased if mAP and HR are determined simply through a balance between impaired sympathetic nervous function and intact parasympa-

thetic nervous function in the mutant mice. Elevated mAP and HR in mutant mice are not attributable to elevated noradrenaline in plasma or to up-regulation of β-adrenergic receptors, as seen in sympathetic denervation, inasmuch as our experiments indicate that the plasma norepinephrine level in wild mice (812 ± 196 pg/ml, $n = 5$) is not significantly different from that of mutant mice (680 ± 255 pg/ml, $n = 5$) and that the agonist and antagonist sensitivities of β-receptors in atrial muscles are similar in wild-type and mutant mice (see above). The elevation of mAP in mutant mice may be due to activation of the renin–angiotensin system, up-regulation of endothelin release, or increased sensitivity of α_1-adrenergic receptors in the central nervous system. It is known that many patients suffering from primary autonomic failure show supine hypertension in addition to orthostatic hypotension (46, 47). The mechanism of supine hypertension has not been fully clarified yet. However, it should be interesting to examine whether attenuation of sympathetic activity by down-regulation of N-type VDCCs can be a cause of primary autonomic failure, because the N-type VDCC null mice showed hypertension (Fig. 4) and lack of baroreflex (Fig. 5). Furthermore, these mice could be useful for the study of renal or pancreatic function, because the functions of these tissues are thought to be strongly dependent on sympathetic nervous activity. Indeed, in insulin-dependent patients with type 1 diabetes mellitus, abnormal sympathetic nervous system function is associated with the progression of renal dysfunction (48). Thus, the N-type VDCC-deficient mouse is expected to be a useful system for studying autonomic failure.

1. Ertel, E. A., Campbell, K. P., Harpold, M. M., Hofmann, F., Mori, Y., Perez-Reyes, E., Schwartz, A., Snutch, T. P., Tanabe, T., Birnbaumer, L., *et al.* (2000) *Neuron* **25,** 533–535.
2. Olivera, B. M., Gray, W. R., Zeikus, R., McIntosh, J. M., Varga, J., River, J., Santos, V. & Cruz, L. J. (1985) *Science* **230,** 1338–1343.
3. Dubel, S. J., Starr, T. V. B., Hell, J., Ahlijanian, M. K., Enyeart, J. J., Catterall, W. A. & Snutch, T. P. (1992) *Proc. Natl. Acad. Sci. USA* **89,** 5058–5062.
4. Williams, M. W., Brust, P. F., Feldman, D. H., Patthi, S., Simerson, S., Maroufi, A., Macue, A. F., Velicelebi, G., Ellis, S. B. & Harpold, M. M. (1992) *Science* **257,** 389–395.
5. Fujita, Y., Mynlieff, M., Dirksen, R. T., Kim, M. S., Niidome, T., Nakai, J., Friedrich, T., Iwabe, N., Miyata, T., Furuichi, T., *et al.* (1993) *Neuron* **10,** 585–598.
6. Coppola, T., Waldmann, R., Brosotto, M., Heurteaux, C., Romey, G., Mattei, M. G. & Lazdunski, M. (1994) *FEBS Lett.* **338,** 1–5.
7. Tanaka, O., Sakagami, H. & Kondo, H. (1995) *Mol. Brain Res.* **30,** 1–16.
8. Whorlow, S. L., Loiacono, R. E., Angus, J. A. & Wright, C. E. (1996) *Eur. J. Pharmacol.* **315,** 11–18.
9. Mills, L. R., Niesen, C., So, A. P., Carlen, P. L., Spigelman, I. & Jones, O. T. (1994) *J. Neurosci.* **14,** 6815–6824.
10. Takemura, M., Fukui, H., Tohyama, M. & Wada, H. (1989) *Neuroscience* **32,** 405–416.
11. Westenbroek, R. E., Hell, J. W., Warner, C., Dubel, S. J., Suntch, T. P. & Catterall, W. A. (1992) *Neuron* **9,** 1099–1115.
12. Westenbroek, R. E., Hoskins, L. & Catterall, W. A. (1998) *J. Neurosci.* **18,** 6319–6330.
13. Bruke, S. P., Adams, M. E. & Taylor, C. P. (1993) *Eur. J. Pharmacol.* **238,** 383–386.
14. Luebke, J. I., Dunlap, K. & Turner, T. J. (1993) *Neuron* **11,** 895–902.
15. Wessler, I., Dooley, D., Werhand, J. & Schlemmer, F. (1990) *Naunyn-Schmiedeberg's Arch. Pharmacol.* **341,** 288–294.
16. Woodward, J., Rezazadeh, S. M. & Leslie, S. W. (1988) *Brain Res.* **475,** 141–145.
17. Herdon, H. & Nahorski, S. R. (1989) *Naunyn-Schmiedeberg's Arch. Pharmacol.* **340,** 36–40.
18. Turner, T. J., Adams, M. E. & Dunlap, K. (1993) *Proc. Natl. Acad. Sci. USA* **90,** 9518–9522.
19. Dooley, D. J., Lupp, A., Hertting, G. & Osswald, H. (1988) *Eur. J. Pharmacol.* **148,** 261–267.
20. Horne, A. L. & Kemp, J. A. (1991) *Br. J. Pharmacol.* **103,** 1733–1739.
21. Komuro, H. & Rakic, P. (1992) *Science* **257,** 806–809.
22. Hirning, L. D., Fox, A. P., McCleskey, E. W., Olivera, B. M., Thayer, S. A., Miller, R. J. & Tsien, R. E. (1988) *Science* **239,** 57–61.
23. Malmberg, A. & Yaksh, T. Y. (1994) *Pain* **60,** 83–90.
24. Toth, P. T., Bindokas, V. P., Bleakman, D., Colmers, W. F. & Miller, R. J. (1993) *Nature (London)* **364,** 635–639.
25. Yamazaki, T., Kawada, T., Akiyama, T., Kitagawa, H., Takauchi, Y., Yahagi, N. & Sunagawa, K. (1997) *Brain Res.* **761,** 329–332.
26. Yahagi, N., Akiyama, T. & Yamazaki, T. (1998) *J. Auton. Nerv. Syst.* **68,** 43–48.
27. Vega, T., Pascul, R. D., Bulbena, O. & Garcia, A. G. (1995) *Eur. J. Pharmacol.* **276,** 231–238.
28. Hong, S. J. & Chang, C. C. (1995) *Br. J. Pharmacol.* **116,** 1577–1582.
29. Seron, A. P. & Angus, J. A. (1999) *Br. J. Pharmacol.* **127,** 927–934.
30. Pruneau, D. & Angus, J. A. (1990) *J. Cardiavasc. Pharmacol.* **16,** 657–680.
31. Williams, M. K., Feldman, D. H., McCue, A. F., Brenner, R., Velicelebi, G., Ellis, S. B. & Harpold, M. M. (1992) *Neuron* **8,** 71–84.
32. Aosaki, T. & Kasai, H. (1989) *Pflügers Arch.* **414,** 150–156.
33. Jun, K., Piedras-Renteria, E. S., Smith, S. M., Wheeler, D. B., Lee, S. B., Han, W., Adams, M. E., Scheller, R. H., Tsien, R. W. & Shin, H. S. (1999) *Proc. Natl. Acad. Sci. USA* **96,** 15245–15250.
34. Saegusa, H., Kurihara, T., Zong, S., Minowa, O., Kazuno, A., Han, W., Matsuda, Y., Yamanaka, H., Osanai, M., Noda, T., *et al.* (2000) *Proc. Natl. Acad. Sci. USA* **97,** 6132–6137. (First Published May 9, 2000; 10.1073/pnas.100124197)
35. Seisenberger, C., Specht, V., Welling, A., Platzer, J., Pfeifer, A., Kuhbandner, S., Striessnig, J., Klugbauer, N., Feil, R. & Hofmann, F. (2000) *J. Biol. Chem.* **275,** 39193–39199.
36. Platzer, J., Engel, J., Schrott-Fischer, A., Stephan, K., Bova, S., Chen, H., Zheng, H. & Stressnig, J. (2000) *Cell* **102,** 89–97.
37. Yagi, T., Tokunaga, T., Furuta, Y., Nada, S., Yoshida, M., Tsukada, T., Saga, Y., Takada, N., Ikawa, Y. & Aizawa, S. (1993) *Anal. Biochem.* **214,** 70–76.
38. Wakamori, M., Yamazaki, K., Matsunodaira, H., Teramoto, T., Takana, I., Niidome, T., Sawada, K., Nishizawa, Y., Sekiguchi, N., Mori, E., *et al.* (1998) *J. Biol. Chem.* **273,** 34857–34867.
39. Kagaya, T., Kajiwara, A., Nagato, S., Akasaka, K. & Kubota. (1996) *J. Pharmacol. Exp. Ther.* **278,** 243–251.
40. Bond, A. & Boot, J. R. (1992) *Eur. J. Pharmacol.* **218,** 179–181.
41. Kirchheim, H. R. (1976) *Physiol. Rev.* **56,** 100–177.
42. Cohn, J. N., Levine, T. B., Olivari, M. T., Garberg, V., Lura, D., Francis, G. S., Simon, A. B. & Rector, T. (1984) *N. Engl. J. Med.* **311,** 819–823.
43. Lechat, P., Packer, M., Chalon, S., Cucherat, M., Arab, T. & Boissel, J. P. (1998) *Circulation* **98,** 1184–1191.
44. Pattyn, A., Morin, X., Cremer, H., Goridis, C. & Brunet, J. F. (1999) *Nature (London)* **399,** 366–370.
45. Thomas, S., Matsumoto, A. M. & Palmiter R. D. (1995) *Nature (London)* **374,** 643–646.
46. Shannon, J., Jordan, J., Costa, F., Robertson, R. M. & Biaggioni, I. (1997) *Hypertension* **30,** 1062–1067.
47. Vagaonescu, T. D., Saadia, D., Tuhrim, S., Phillips, R. A. & Kaufmann, H. (2000) *Lancet* **355,** 725–726.
48. Weinrauch, L. A., Kennedy, F. P., Gleason, R. E., Keough, J. & D'Elia, J. A. (1998) *Am. J. Hypertens.* **11,** 302–308.